J Infrared Milli Terahz Waves (2014) 35:525–535
DOI 10.1007/s10762-014-0068-x

Analysis of square Fresnel Zone Plate Lens for dual band detectors

D. Etayo · I. Ederra · R. Gonzalo

Received: 22 July 2013 / Accepted: 19 March 2014 /
Published online: 13 April 2014

Abstract Dust emission is used in space applications for star-formation characterization normally acquired by different detectors operating at Infrared (IR) and sub-millimeter wave (sub-mm wave) frequencies. An integrated dual band detector working at both frequency ranges is described in this paper. The proposed configuration implements a spiral antenna working at sub-millimeter wave frequencies whose design is based on Fresnel zones theory. At the same time, this spiral antenna is used as Fresnel lens to focus IR power (12 μm) into an IR detector. The paper describes the influence of implementing a sub-mm wave spiral antenna based on square Fresnel zones. In particular, the effects on the focal distance and the focal gain at IR frequencies and the radiation features at sub-mm wave frequencies are studied. Furthermore, the importance of the number of Fresnel zones used in the design of the sub-mm spiral antenna is also determined.

Keywords Sub-millimetre wave frequencies · Fresnel Zones · infrared · spiral antennas

1 Introduction

The star formation process is characterized by the presence of a huge amount of warm and cold dust, whose emission ranges mainly from infrared to millimeter wavelengths. Therefore, the early stages of stellar evolution are characterized by dust emission peaking at wavelengths in the range 4-100 μm. A detector that can work simultaneously at far-IR wavelengths, and at sub-millimeter wavelengths, would be very useful to study the physical conditions in the different stages of the star formation process and also for general space exploration [1, 2].

Such a detector in a single observation would provide data at both sides of the dust emission peak, covering simultaneously a wavelength range where the emission is optically thick (the electrical size of the dust emission is larger than the wavelength) and another where the emission becomes optically thin (the electrical size of the emission is comparable to the wavelength). Therefore, these two wavelength regimes provide complementary information on the emitting material, which is most useful for the models to better constrain the physical parameters of the objects.

D. Etayo (✉) · I. Ederra · R. Gonzalo
Antenna Group. Electric and Electronic Department, Public University of Navarra,
31006 Pamplona, Navarra, Spain
e-mail: david.etayo@unavarra.es

So far, these kinds of observations have been carried out using a different instrument in each wavelength regime. Therefore, the observational uncertainties in each operational regime had a different nature due to the use of different instrumentation. Using the same instrument to obtain data simultaneously in the far-IR and sub-mm waves will simplify the calibration and would allow minimizing of observational uncertainties. Also, the possibility of simultaneous far-IR and sub-mm observations would save observing time.

The objective of this work is to develop and analyze an integrated dual band detector operating at sub-mm and IR frequencies based on the use of a non-ideal Fresnel Zones Plate Lens (FZPL) [3, 4]. Similar configurations have been proposed and studied in the IR and visible ranges [4]. However, their use for sub-mm detection is more challenging, due to the larger frequency difference between both bands. Moreover, submillimeter wave detectors are usually built with discrete components, e.g. diodes, which are large in terms of the wavelength. This imposes some constraints in the design. In this paper, the additional problems of the sub-mm wave antenna design are eliminated by the use of the theory of FZPL. The proposed configuration is suitable to operate at both frequency bands; i.e., sub-mm wave and IR with good performances.

The paper is structured as follows. After a short description of the preliminary design of the detector (Section 2), the design of the Fresnel Zone Plate Lens is reported in Section 3. The influence of using non-ideal Fresnel Zones (FZ) on the focal gain and focal distance of the FZPL at IR frequencies is studied in Section 4. The performances of the antenna at submillimeter wave frequencies are presented in Section 5. Finally, in Section 6, the conclusions are drawn.

2 System configuration description

The proposed dual band configuration consists of a planar spiral antenna and an IR detector, as it is shown in Fig. 1. Both of them are mounted in a Silicon (Si) substrate. The spiral antenna placed on the top of the Si substrate is designed to operate at sub-millimeter wave frequencies, in particular around 450 GHz [5]. This antenna results from a conversion of an ideal FZPL to a quasi-spiral antenna [6]. As FZPL, it focuses, at the same time, the incoming IR radiation into the IR detector, which is placed at the bottom of the Si substrate, as depicted in Fig. 1. For this design, the FZPL has been designed to operate in the IR regime at 12 μm (25 THz).

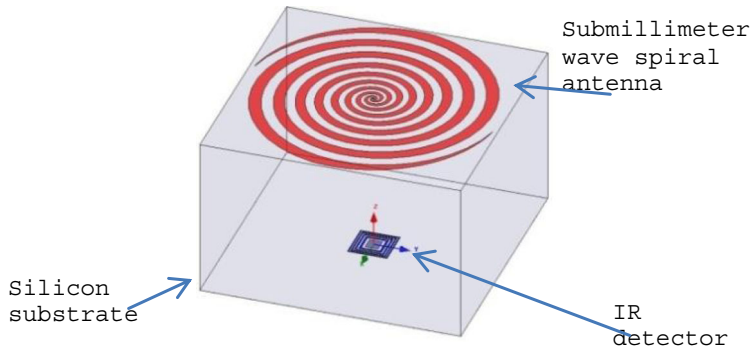

Fig. 1 Schematic of the proposed THz-IR receiver

3 Fresnel Zone Plate design

The radii of the Fresnel zones used for FZPL design [4] are calculated using Equation (1). They depend on the wavelength, the material used as substrate and the focal distance.

$$r_m = \left(m d_0 \frac{\lambda_0}{n} \right)^{1/2} \tag{1}$$

where r_m is the radius of the m-Fresnel Zone; m, the Fresnel Zone index; d_0 is the focal distance; λ_0 is the wavelength at working frequency and n is the refractive index of the substrate, in this case silicon.

The circular rings of the Fresnel lens must be transformed into a quasi-spiral in order to act as sub-mm wave antenna. This must be done by connecting adjacent rings. These connecting sections degrade its performance as antenna, and therefore, the use of a square FZ lens seems to be more suited for the final design.

Therefore an approximation to square FZ was carried out using Equation (2).

$$x_m = \frac{r_m \sqrt{\pi}}{2} \tag{2}$$

where r_m is the radius of the circular FZ and x_m is half length of the adapted square FZ. Moreover, square FZPLs are better matched to the intrinsic geometry of a rectangular array of receivers [7].

On the other hand, it is important to point out that a Schottky diode will be used as sub-mm wave detector. Therefore, its size will impose a size condition in the implementation of the FZPL. In fact, the size of the first Fresnel Zone has to be at least 100 x 100 μm^2 (for a circular area larger than 10000 μm^2, $r_1 > 57$ μm) in order to have enough space to place a Virginia Diode (VDI) [8] diode in the central point of the square spiral antenna (see Fig. 2). Taking this

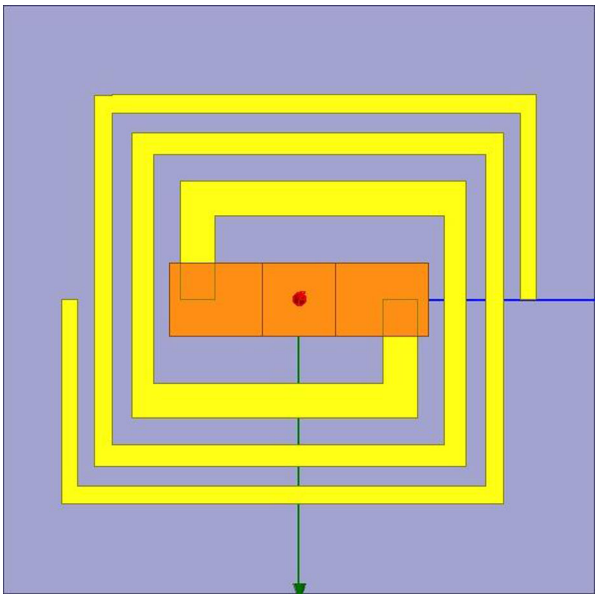

Fig. 2 Sub-millimeter Wave Antenna (yellow) and detector diode (orange). Note that the spiral antenna depicted is made with 8 FZ

into account the Fresnel lens is designed for an ideal focal distance of 1000 μm using Eq. (1). Note that for d_0=1000 μm, the radius of the first Fresnel zone is r_1=59.2 μm which is larger than 57 μm, as required. Finally, using Eq. (2) to calculate the size of the square Fresnel Zone, a value of x_1=52.5 μm is obtained. The relationship between the values to the ideal radius of the FZ and the ones of the square zones are presented in Table 1. The latter ones will be used to design the Fresnel Zone Plate sub-mm wave antenna.

Due to the use of a finite number of FZ and the square shape of the spiral sub-mm wave antenna, both its focusing performances as IR lens and its radiation properties at sub-mm wave frequencies will be affected. Simulation results and theoretical expression [9, 10] show that sharp corners (bends) have more influence than smooth circular paths on the propagation of electromagnetic fields due to reflections caused by the change in the characteristic impedance that they introduce. On the other hand, smooth circular paths do not introduce this change, and therefore, the transformation from circular to square FZ affects the performances of the FZPL working as submillimeter-wave antenna. These effects will be analyzed in the next sections.

Note that the metal rings used for the implementation of the FZPL are obtained subtracting to the n-th even zones the previous odd zone (zone n-1). Thus, the external radius of each metal FZ corresponds with the radius of the even zones and the inner radius is given by the odd zones. Following this procedure, the minimum spacing obtained is 6.7 μm and the maximum spacing is 21.7 μm.

4 Fresnel Zone Plate Lens IR performances

Once the limitation of the first Fresnel zone has been considered in the design, it is important to determine, the real focal distance of the FZPL taking into account the use of square spirals; and the focal gain obtained as a function of the number of Fresnel zones used in the design of the sub-mm wave square spiral antenna.

Table 1 Fresnel Zones size

Zone number	Circular FZ Radius (μm)	Square FZ Half Side (μm)
1	59.2	52.5
2	83.8	74.2
3	102.6	90.9
4	118.5	105.0
5	132.5	117.4
6	145.1	128.6
7	156.7	138.9
8	167.5	148.5
9	177.7	157.5
10	187.3	166.0
11	196.5	174.1
12	205.2	181.8
13	213.6	189.3
14	221.6	196.4
15	229.4	203.3
16	236.9	210.0

In order to check its IR performances when square FZ are employed, seven different square antenna configurations were analyzed; all the even cases from 4 to 16 FZ. The study was carried out with Ansys-HFSS software [11]. Note that no more than 16 Fresnel zones have been taken into account in the design due to the resolution of the available photolithographic process in our laboratory, which is limited to 5 μm. With these constrains, it is difficult to fabricate the 18FZ-antenna because the gap in between the 16^{th} FZ and the 18^{th} FZ is close to 6 μm.

An incident plane wave (negative z-axis propagation direction) has been used as an excitation. The analysis has been limited to linear polarization, so that, the incident plane wave has a linear polarization along the x-axis. Note that due to its symmetry the FZPL presents a similar behavior for both linear polarizations (x-axis and y-axis). Furthermore, in order to have enough simulation resources (memory requirements), only a thin region of the structure has been simulated, as it is depicted in Fig. 3 (lower row). This region is a transversal cut, defined from the lens central axis (x-axis) to the external face (the final volume simulated is 400 μm x 5 μm x 1000 μm). In this case, symmetry boundary conditions have been defined in both side faces. This approach is adequate to determine the properties of the structure as a lens.

Fig. 3 (upper row) shows a comparison between the performances of the sub-mm wave antenna acting as lens implemented with ideal (i.e. circular) FZ and with square FZ operating at the IR frequency (12 μm). This Figure shows the propagation of the electric field magnitude through the Si substrate where the lens is implemented. In both cases, 16 FZs are used to form the sub-mm wave antenna.

The magnitude of the electric field focuses at 1000 μm for the case of circular Fresnel zones (Fig. 3a). On the other hand, square Fresnel zones (Fig. 3b) focus the electric field at a shorter distance. This result shows an important shifting of the focal distance due to the transformation from circular to square of the Fresnel zones.

Note that there is a small fraction of the electric field that is not focused by the FZPL, as it is clearly depicted in Fig. 3b and will be studied later on. Note that the value of this fraction decreases as the area of the FPZL increases.

To analyze the displacement of the focal point and to obtain the focal distance for the square FZ, the maximum amplitude along the z-axis of the magnitude of the electric field within the silicon substrate for the different number of analyzed FZs is depicted in Fig. 4. Note that 0 μm position represents the point where the FZPL is located.

As it is depicted in Fig. 4, it can be concluded that the maximum of the electric field using square Fresnel zones is concentrated around 800 μm instead of the ideally expected 1000 μm. This result clearly shows that the focal distance is affected by the shape of the FZs. For the sake of simplicity, only FZPLs made with 12, 14 and 16 FZs are depicted.

On the other hand, if the number of FZ is increased, the magnitude of the electric field at the focus point is expected to be increased. For the sake of representation, the ratios between the magnitude of the electric field at the focal point for the cases with and without a FPZL are calculated (Gain Factor). This ratio is defined as follows;

$$\mathrm{GF} = \frac{\textit{Electric Field with FPZL}}{\textit{Electric Field without FPZL}} \tag{3}$$

This Gain Factor at the bottom of the Si substrate (along the x axis for z=800 μm) for each analyzed square FZPL is shown in Fig. 5. Note that the same substrate volume (400 μm x 5 μm x 800 μm) has been used for each simulation. Excitation and boundary conditions

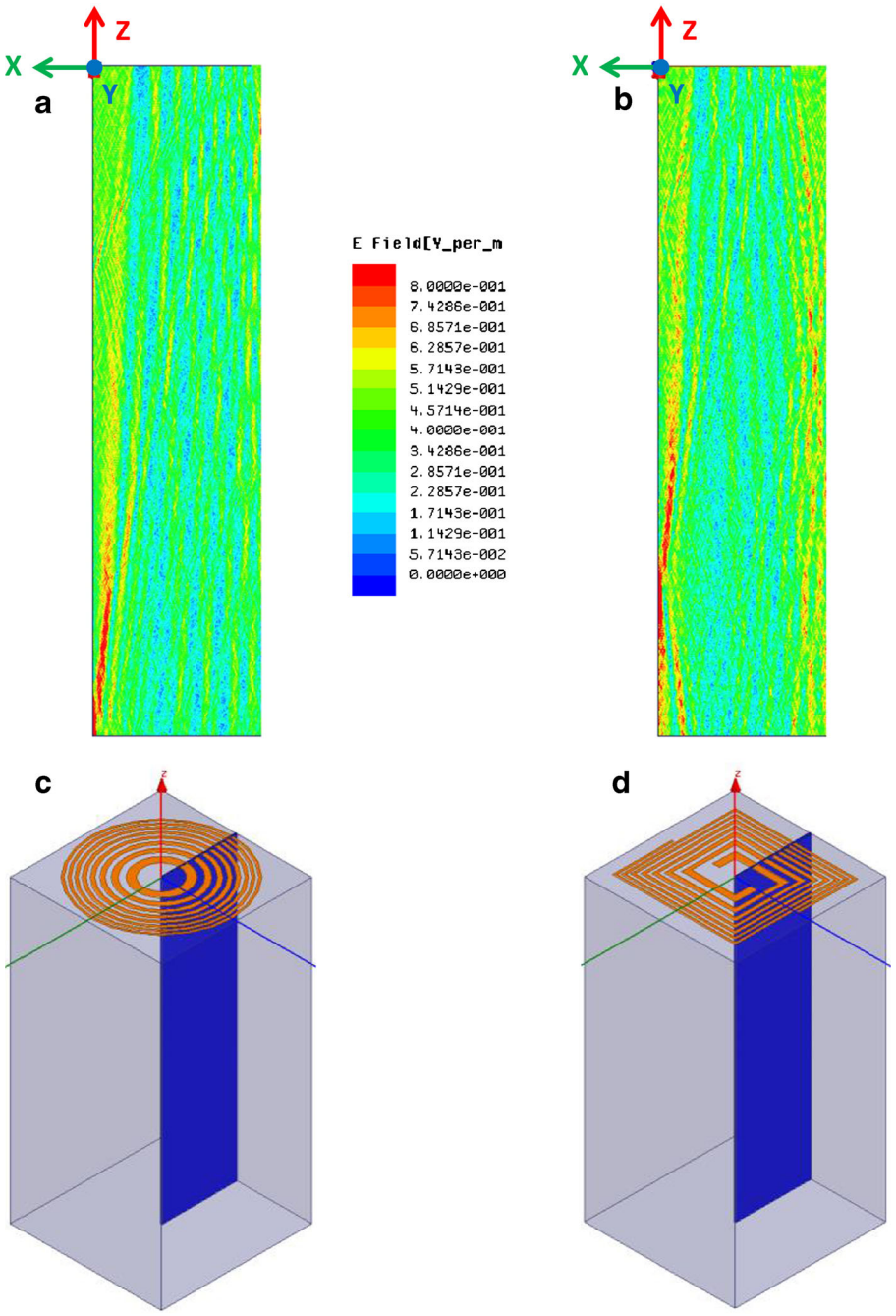

Fig. 3 Comparison of the magnitude of the electric field between (a) 16 circular Fresnel zones and (b) 16 square Fresnel zones. Note that only half of the substrate is depicted in the upper row. In the lower row, a full view of each device is depicted. The simulation slice is marked in blue

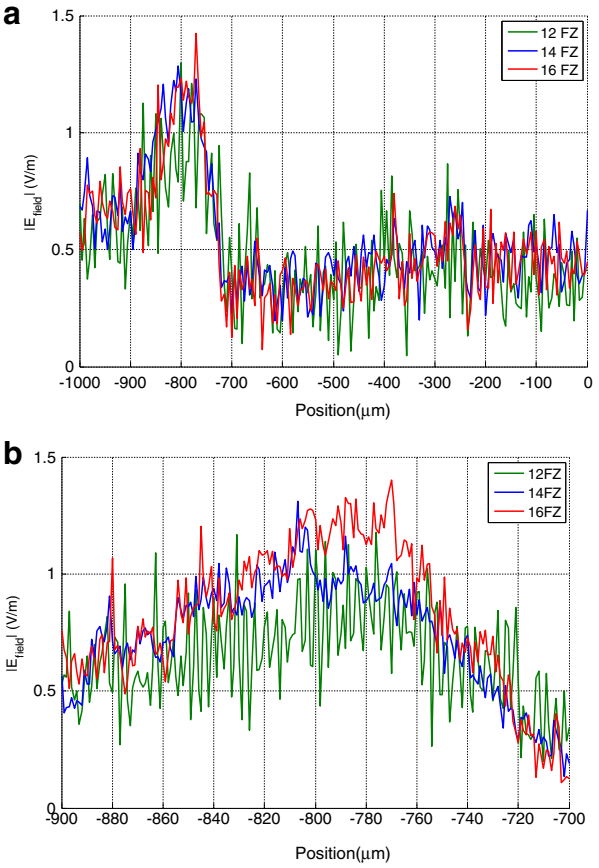

Fig. 4 (a) Amplitude distribution of the electric field within the silicon substrate. 0 μm corresponds with the sub-mm wave antenna position. λ=12 μm and (b) zoom around 800 μm

(incident plane wave and symmetry boundary conditions) are the same as in the previous cases. The FZPL formed by 16 Fresnel zones exhibits the maximum Gain Factor which is close to 4.5 (the magnitude of the electric field obtained using the FZPL is 4.5 times higher than the case of no lens).

Note that the small fraction of the electric field flowing at the edge of the Si substrate which was previously noticed (Fig. 3b) has no influence in the focalization gain, as seen in Fig. 5, i.e. the maximum value of the power is concentrated around 0 μm.

Fig. 6 summarizes the maximum value of the Gain Factor for each FZ antenna analyzed in Fig. 5. Furthermore, the maximum value of the theoretical Gain Factor for circular Fresnel Zones has also been depicted for comparison issues. For this analysis, the number of FZ has been extended from 4 FZ to 50 FZ.

In this figure, it can be noted that the circular FZL theoretical Gain Factor (CFZ) is higher than the square FZ (SFZ) for all the cases. Note that both curves present a similar trend. It is important to remark that the focal distance for the SFL is 800 μm. This value, as the number of Fresnel zones increases, saturates to a constant value; i.e., 6.5 and 5.7 for CFZ and SFZ zones respectively. Note that its trend will depend on the focal distance [12].

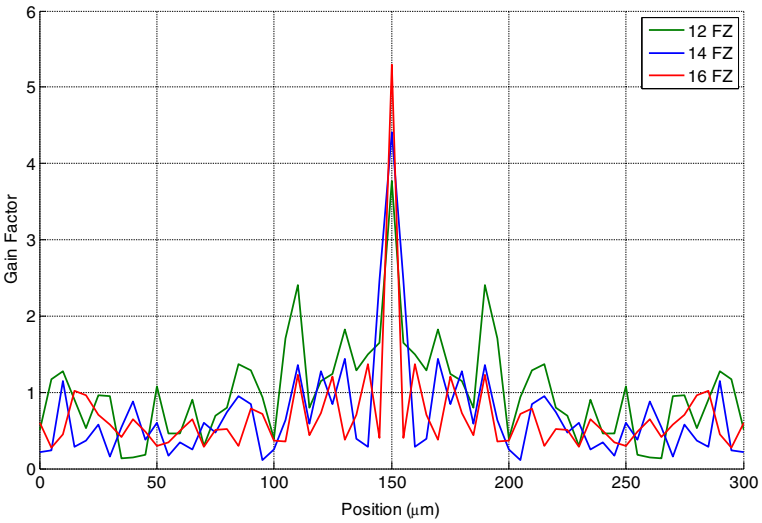

Fig. 5 Gain Factor value as function of the number of square Fresnel Zones along the x axis for z=800 μm. Operational wavelength of 12 μm

5 Submillimeter wave antenna performances

In the previous section, the study of the focal distance and the GF for the Fresnel Zone Plate Lens, working at 12 μm has been presented. In this section, the study of its performance as a sub-millimeter wave antenna, operating at 450 GHz, is described.

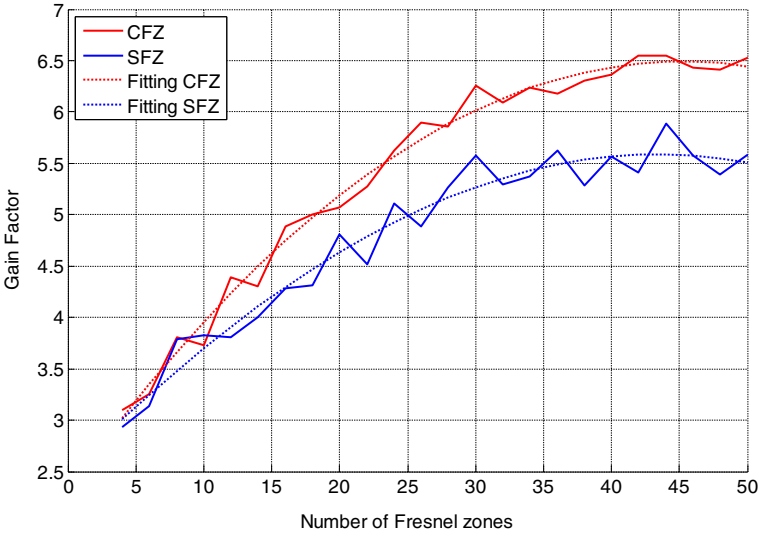

Fig. 6 Gain Factor for each antenna at 800 μm. CFZ is calculated for Circular Fresnel Zones and SFZ for square Fresnel Zones

For analyzing the sub-mm antenna radiation performances, a lumped port has been defined as excitation port (central square area in Fig. 2). This excitation models the diode that will be used as detector in the final implementation. Note that the size, W, and the input impedance, Z_{diode}, of the simulated diode are obtained from a commercial VDI diode [8] (Z_{diode}=15 Ω at 427 GHz, W=30 μm, and a total length of 150 μm).

To simulate the model, symmetric boundary conditions have been defined in both side faces to replicate an infinite array [11]. Furthermore, the top/bottom faces of the structure have been designated as radiation boundary condition. The size of the Si substrate is 500 μm x 500 μm x 800 μm.

In Fig. 7, the reflection coefficient (S_{11} parameter) of the square spiral antenna is depicted. The values for the 4-6FZ antennas have been not included due to their low GF value. The results show two antenna working bands, around 210 GHz and 427 GHz.

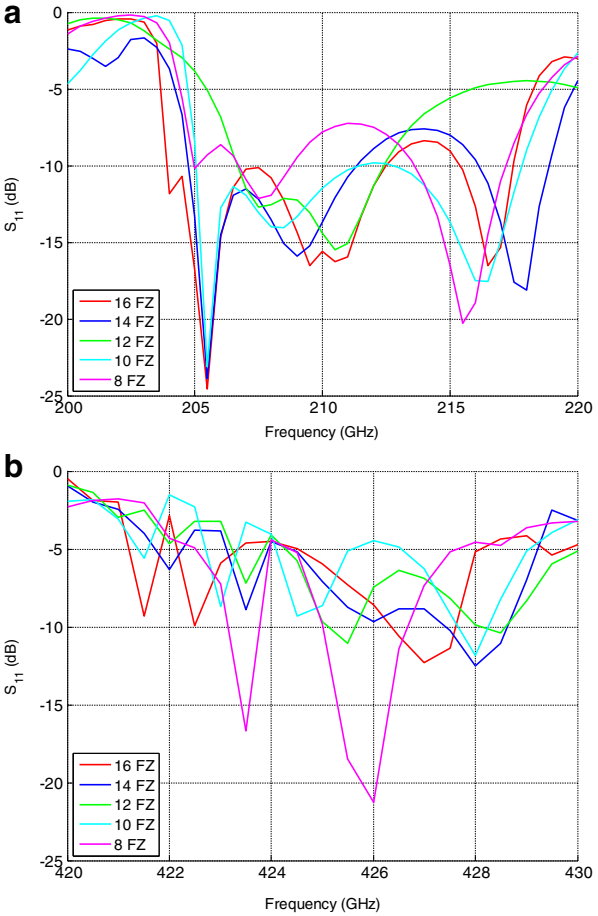

Fig. 7 S_{11} parameter of the sub-mm wave antennas working at (a) 210 GHz and (b) 427 GHz

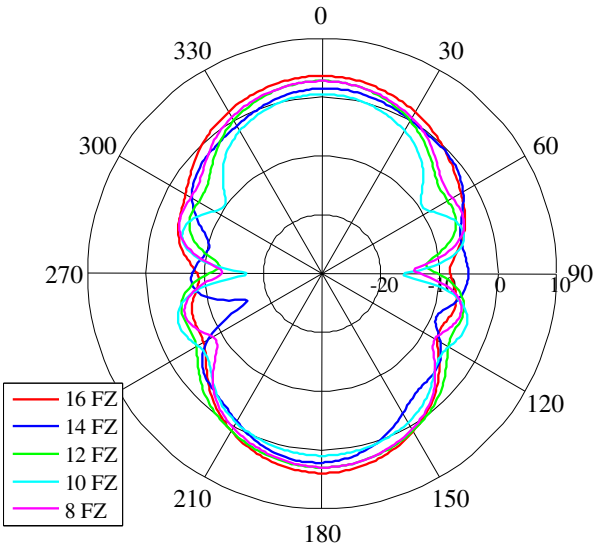

Fig. 8 Directivity of the square antennas at 427 GHz

The simulated S_{11} parameter is better than -5 dB from 424 GHz to 430 GHz for most of the simulated sub-mm square spiral antennas. In the lower band, the scattering S_{11} parameter is better than -7 dB from 205 to 215 GHz.

Finally, the directivity pattern of the square spiral antennas is shown in Fig. 8. Note that due to the fact that the sub-mm wave antenna is placed on a Si substrate, more power is trapped by the substrate than radiated to free space, and therefore, the back radiation is higher than the front one (see Theta=±180º versus 0º).

The maximum value of the directivity is obtained for the case of 16-FZ square spiral sub-mm antenna, which has a value larger than 3 dBi.

6 Conclusions

The design of a submillimeter wave antenna, operating at 427 GHz, which also acts as Fresnel Zone Plate Lens at IR frequencies (12 μm), has been presented. The sub-mm wave antenna resulted from a transformation of a Fresnel Zone Plate Lens.

The influence of the number of FZ used to implement the submillimeter wave antenna on the IR power focalization has been studied for the case of linear polarization. As the number of FZ forming the sub-mm wave antenna increases, the gain factor also enlarges. A Gain Factor improvement of 4.5 times has been obtained with the implementation of 16 FZs. Furthermore, the shifting of the focal point due to the square shape of Fresnel Zones used to implement the Fresnel Zone Plate Antenna has also been investigated. The antenna exhibits reasonable performances operating at sub-mm wave frequencies with a S_{11} parameter below -5 dB (from 424 to 428 GHz) and a directivity of 3.6 dBi (f=427 GHz).

Acknowledgment This work was supported by the Spanish Ministry of Economy and Competitiveness Project Nos. TEC-2009-11995 and CSD 2008-00066.

References

1. Rao K.N., Webler A. Spectroscopy of the Earth's Atmosphere and Interstellar Medium (Academic Press, Boston, 1992).
2. De Maagt P. Int Antenna Technol Workshop: Small Smart Antennas Metamater Applicat (2007) doi:10.1109/IWAT.2007.370091.
3. González F.J., Ilic B., Aida J., Boreman, G.D. IEEE J Quantum Electron (2005) doi:10.1109/JSTQE.2004.841474.
4. González F.J. and Alda J Opt Lett (2009) doi:10.1364/OL.34.000809
5. Brown E.R., Lee A.W.M., Navi B.S., Bjamason J.E. Microw Opt Techn Let (2006) doi:10.1002/mop.21398.
6. González F.J., Alda J., Ilic B., Boreman, G.D. Appl Optics (2004) doi:10.1364/AO.43.006067.
7. Minin I.V., Minin O.V., Basic Principles of Fresnel Antenna Arrays. (Springer Berlin Heidelberg 2008).
8. Virginia Diodes http://vadiodes.com/. Accessed 12 September 2013.
9. Mao J., Xu Y., Zhang R., Yang M. and Liu J. Int Conf Microwave Tec Comput Electrom (2009) doi:10.1049/cp.2009.1309.
10. Sato N., Kitagawa J., Kadoya Y.J Infrared Millim W. (2011) doi:10.1007/s10762-010-9681-5.
11. Ansys HFSS 13 http://www.ansoft.com/. Accessed 12 September 2013
12. O. V. Minin, I. V. Minin. Diffractive Optics of Millimetre Waves. (IOP Publisher, Boston-London, 2004).